PERGAMON

International Journal of Solids and Structures 38 (2001) 8945–8960

INTERNATIONAL JOURNAL OF SOLIDS and STRUCTURES

www.elsevier.com/locate/ijsolstr

Shear band development predicted by a non-normality theory of plasticity and comparison to crystal plasticity predictions

Mitsutoshi Kuroda [a,*], Viggo Tvergaard [b]

[a] *Department of Mechanical Systems Engineering, Yamagata University, 4-3-16 Jonan, Yonezawa, Yamagata 992-8510, Japan*
[b] *Department of Mechanical Engineering, Solid Mechanics, Technical University of Denmark, Building 404, DK-2800 Lyngby, Denmark*

Received 19 April 2001

Abstract

A phenomenological plasticity model has recently been proposed, which combines a smooth yield surface for an anisotropic solid with a vertex-type plastic flow rule. Both polycrystal plasticity calculations and experiments have shown the type of non-normality of plastic flow, which is represented by this material model. The plasticity model is here implemented in a finite element programme and is used to analyze the plane strain tensile test, thus representing the formation of a neck and the subsequent evolution of shear bands in the neck region. To test the predictions of the phenomenological plasticity model the tensile test problem is also analyzed by polycrystal plasticity, based on the Taylor model for either b.c.c. or f.c.c. crystal structure. It is shown that the phenomenological plasticity model gives a good approximation of the crystal plasticity predictions. © 2001 Elsevier Science Ltd. All rights reserved.

Keywords: Strain localization; Constitutive equation; Polycrystalline metals; Finite strain; Finite element method

1. Introduction

The use of an abrupt strain path change to determine the shape of the subsequent yield surface in the vicinity of a current loading point has been proposed by Kuroda and Tvergaard (1999). The abrupt strain path change forces the stress point to move rapidly along the current yield surface, and when the method was applied to polycrystal plasticity, based on the Taylor model for either f.c.c. or b.c.c. crystal structure, a clear non-normality of the small amount of plastic flow was predicted. It was pointed out (Kuroda and Tvergaard, 1999) that this apparent non-normality must be a vertex-type effect resulting from the Taylor model, since normality of each of the slip systems involved is an integral part of the crystal plasticity model.

* Corresponding author. Tel.: +81-238-26-3211; fax: +81-238-26-3205.
E-mail address: kuroda@dip.yz.yamagata-u.ac.jp (M. Kuroda).

0020-7683/01/$ - see front matter © 2001 Elsevier Science Ltd. All rights reserved.
PII: S0020-7683(01)00166-4

Thus, part of the explanation of this predicted vertex-type effect is that the proposed method gives a yield surface larger than that corresponding to a very small offset, in agreement with the assumption always used in plasticity models in practice. In a recent experimental investigation for an aluminum alloy and a steel (Kuwabara et al., 2000) the abrupt strain path change was also used, and these experimental measurements showed a clear non-normality of the plastic strain rate vector relative to the stress path, much like that predicted in the crystal plasticity studies.

To include these predicted and experimentally observed non-normality effects in a phenomenological plasticity model, Kuroda and Tvergaard (2001a) have recently proposed a material model that combines a smooth yield surface for an anisotropic solid with a vertex-type plastic flow rule. The prediction of plastic instabilities is a very good test of such a material model, since it is well known that here a vertex has a big effect (Støren and Rice, 1975; Hutchinson and Tvergaard, 1981; Needleman and Tvergaard, 1982). Therefore, the new material model was tested on the prediction of the onset of necking in biaxially stretched metal sheets, using the relatively simple M–K-type model that assumes uniform straining outside the localized band. It was found that the critical strains predicted by the proposed material model are quite realistic, also in the range of equi-biaxial stretching where the normality flow rule leads to unrealistically late instabilities, and thus the predicted forming limit diagrams are much like those found for J_2 corner theory of plasticity (Christoffersen and Hutchinson, 1979) or for crystal plasticity.

For the somewhat different purpose of developing efficient computational procedures, Hughes and Shakib (1986) have suggested using a load-direction-dependent plastic modulus, and Simo (1987) has proposed a plasticity model for which a non-associative flow rule on a Mises yield surface is used to represent a corner-like effect. It is noted that the tensorial form of the plastic flow rule used in the non-normality theory (Kuroda and Tvergaard, 2001a,b) was motivated by the proposition of Simo (1987), but a modification was made so that the non-normality (corner-like) behavior is reasonably consistent with that inherently involved in crystal plasticity. The non-normality theory (Kuroda and Tvergaard, 2001a,b) is not only simpler than the J_2 corner theory (Christoffersen and Hutchinson, 1979; also see the review by Neale (1981)), but can also account for strain-rate sensitivity and plastic anisotropy.

Other corner theories have been proposed, e.g. Gotoh (1985) and Hu et al. (1998). These corner theories as well as the J_2 corner theory have incorporated a dependence of the direction of plastic strain rate on that of stress rate, while Simo's and our theories have assumed the dependence of the direction of plastic strain rate on that of total strain rate.

The development of shear bands in a J_2 corner theory material under plane strain conditions has been analyzed by Hutchinson and Tvergaard (1981) and by Tvergaard et al. (1981). It was emphasized, based on the bifurcation study of Hill and Hutchinson (1975), that for a hardening material no shear band instability will be predicted by classical J_2 flow theory with a smooth yield surface and normality. Thus, J_2 corner theory was used to model the vertex formation known from polycrystal plasticity, and it was found that shear bands develop. A numerical study for a tensile test specimen, as that of Tvergaard et al. (1981), has also been carried out for a single crystal directly based on crystal plasticity (Peirce et al., 1983), and also this study has shown the development of shear bands in the neck region.

In the present paper the development of shear bands in the neck of a plane strain tensile test specimen is analyzed, with focus on a direct comparison of predictions based on the non-normality theory of plasticity (Kuroda and Tvergaard, 2001a) and predictions based on crystal plasticity. The non-normality theory is here implemented in a finite element programme, and the elements used are chosen so that there is not a strong sensitivity to the angular orientation of shear bands. The crystal plasticity analyses make use of the Taylor polycrystal model, with many grain orientations represented for each integration point in the finite element approximation of the field quantities, and thus these computations are much more computationally heavy than those based on the non-normality theory.

2. Constitutive models

The results to be presented here are based on either the phenomenological non-normality theory of plasticity or on crystal plasticity using the Taylor polycrystal model. First, the basic equations of the two material models are briefly presented here. In the following, the tensors and vectors will be denoted by boldface letters: for example $\mathbf{a} = a_{ij}\mathbf{e}_i \otimes \mathbf{e}_j$, $\mathbf{b} = b_{ij}\mathbf{e}_i \otimes \mathbf{e}_j$, $\mathbf{n} = n_i\mathbf{e}_i$, where $\otimes$ denotes the tensor product and $\mathbf{e}_i$ a Cartesian basis. The following definitions for operation are used: $\mathbf{ab} = a_{ik}b_{kj}\mathbf{e}_i \otimes \mathbf{e}_j$, $\mathbf{an} = a_{ij}n_j\mathbf{e}_i$, $\mathbf{a} : \mathbf{b} = a_{ij}b_{ij}$, with proper extension to higher order tensors. A superposed dot denotes the (material) time derivative.

2.1. Phenomenological non-normality theory of plasticity

The phenomenological constitutive model considered here is fundamentally the same as that provided in Kuroda and Tvergaard (2001a,b). The basic equations of the model are given below.

Assuming small elastic and finite plastic deformations, we can express the result of the Eulerian kinematics by

$$\mathbf{D} = \mathbf{D}^{\mathrm{e}} + \mathbf{D}^{\mathrm{p}} = \mathbf{D}^{\mathrm{e}} + \dot{\Phi}\mathbf{N}^{\mathrm{p}}, \tag{1}$$

$$\mathbf{W} = \boldsymbol{\omega} + \mathbf{W}^{\mathrm{p}} = \boldsymbol{\omega} + \dot{\Phi}\boldsymbol{\Omega}^{\mathrm{p}}, \tag{2}$$

where $\mathbf{D}$ and $\mathbf{W}$ are the symmetric and anti-symmetric parts of the spatial velocity gradient $\mathbf{L}$ ($= \partial v_i/\partial x_j \mathbf{e}_i \otimes \mathbf{e}_j$ with $\mathbf{v}$ being the velocity of a material particle and $\mathbf{x}$ being its current position), the superscripts e and p denote elastic and plastic parts, $\boldsymbol{\omega}$ is the spin of material substructure, and $\mathbf{N}^{\mathrm{p}}$ and $\boldsymbol{\Omega}^{\mathrm{p}}$ define the direction of $\mathbf{D}^{\mathrm{p}}$ and $\mathbf{W}^{\mathrm{p}}$, respectively. The scalar-valued quantity $\dot{\Phi}$ is a non-negative overstress function for rate-dependent cases (if we consider rate-independent elasto-plasticity, $\dot{\Phi}$ corresponds to a loading multiplier appearing as $\langle\lambda\rangle$, where $\langle\ \rangle$ are the Macauley brackets).

With the superposed $\circ$ denoting an objective rate with respect to the spin $\boldsymbol{\omega}$, the elasticity relation is assumed to be given by Hooke's law

$$\overset{\circ}{\boldsymbol{\sigma}} = \dot{\boldsymbol{\sigma}} - \boldsymbol{\omega}\boldsymbol{\sigma} + \boldsymbol{\sigma}\boldsymbol{\omega} = \mathbf{C} : \mathbf{D}^{\mathrm{e}} = \mathbf{C} : \mathbf{D} - \dot{\Phi}\mathbf{C} : \mathbf{N}^{\mathrm{p}}, \tag{3}$$

where $\boldsymbol{\sigma}$ is the Cauchy stress, $\mathbf{C}$ is a fourth order elastic moduli tensor which is also assumed to be isotropic, determined only by Young's modulus E and Poisson's ratio ν.

The 'dynamic' yield surface is assumed to be given by

$$f = J_{\mathrm{e}}(\boldsymbol{\sigma}, \mathbf{s}_i, \varepsilon^{\mathrm{p}}) - g(\varepsilon^{\mathrm{p}})(\dot{\Phi}/\dot{\Phi}_0)^m = 0, \tag{4}$$

where J_{e} is an equivalent stress for which the functional form may be motivated by a rate-independent theory of plasticity, $\mathbf{s}_i$ represents tensor or vector structure variables, ε^{p} is an equivalent plastic strain, $g(\varepsilon^{\mathrm{p}})$ is a strain hardening function which portrays isotropic hardening, m is a rate sensitivity parameter and $\dot{\Phi}_0$ is a reference value of the overstress function. The expression J_{e} is assumed to be pressure insensitive, i.e. $\partial J_{\mathrm{e}}/\partial\boldsymbol{\sigma} \equiv \mathbf{N}^n$ is a deviatoric quantity.

It is obvious that the function $\dot{\Phi}$ directly corresponds to the magnitude of the plastic strain rate. From Eq. (4) the expression for $\dot{\Phi}$ is determined as

$$\dot{\Phi} = \dot{\Phi}_0(J_{\mathrm{e}}/g)^{1/m}. \tag{5}$$

The unit outward normal $\mathbf{n}$ to the dynamic yield surface is defined as

$$\mathbf{n} = \left(\frac{\partial J_{\mathrm{e}}}{\partial\boldsymbol{\sigma}}\right) \Big/ \left\| \frac{\partial J_{\mathrm{e}}}{\partial\boldsymbol{\sigma}} \right\|, \tag{6}$$

where $\|(\cdot)\| = (\mathrm{tr}[(\cdot)^{\mathrm{T}}(\cdot)])^{1/2}$ with the superscript T denoting 'transpose'. We assume a non-linear dependence of the plastic strain rate $\mathbf{D}^{\mathrm{p}}$ on the total strain rate $\mathbf{D}$, analogous to the expression originally proposed by Simo (1987). Introducing the notation for a deviatoric quantity, $(\cdot)' = (\cdot) - (1/3)(\mathbf{I}\otimes\mathbf{I}) : (\cdot)$, with the unit tensor $\mathbf{I}$, a direction $\mathbf{m}$ normal to $\mathbf{n}$ is defined as

$$\mathbf{m} = \frac{\mathbf{D}' - (\mathbf{n} : \mathbf{D}')\mathbf{n}}{\|\mathbf{D}' - (\mathbf{n} : \mathbf{D}')\mathbf{n}\|}. \tag{7}$$

Then, the direction $\mathbf{N}^{\mathrm{p}}$ of the plastic strain rate $\mathbf{D}^{\mathrm{p}}$ is taken to be

$$\mathbf{N}^{\mathrm{p}} = \mathbf{n} + \hat{\delta}\mathbf{m}, \tag{8}$$

where $\hat{\delta}$ is a scalar-valued function to be specified below. Eq. (8) together with Eq. (1) specifies the model consisting of a smooth dynamic yield surface with a non-normality flow rule, i.e. $\mathbf{D}^{\mathrm{p}} = \dot{\Phi}\mathbf{N}^{\mathrm{p}}$. The equivalent plastic strain ε^{p} is defined as

$$\varepsilon^{\mathrm{p}} = \int \dot{\varepsilon}^{\mathrm{p}}\,\mathrm{d}t = \int \sqrt{2/3}\dot{\Phi}\,\mathrm{d}t. \tag{9}$$

As in Kuroda and Tvergaard (2001a,b), $\hat{\delta}$ is taken to be given by

$$\hat{\delta} = \tan\theta^{\mathrm{p}}, \quad \theta^{\mathrm{p}} = \begin{cases} \alpha\theta & \text{for } \alpha\theta \leqslant \theta^{\mathrm{p}}_{\mathrm{crit}} \\ \theta^{\mathrm{p}}_{\mathrm{crit}} & \text{for } \alpha\theta > \theta^{\mathrm{p}}_{\mathrm{crit}} \end{cases} \tag{10}$$

with

$$\theta = \cos^{-1}\left[\frac{\mathbf{n} : \mathbf{D}'}{\|\mathbf{D}'\|}\right], \tag{11}$$

$$\alpha = \frac{1}{c(g/\mu) + 1}, \tag{12}$$

where c is a coefficient to be determined, which governs non-coaxiality between $\mathbf{D}'$ and $\mathbf{D}^{\mathrm{p}}$, and μ is the elastic shear modulus ($\mu = E/\{2(1+\nu)\}$). The ratio μ/g represents the elastic modulus normalized by the current stress level g according to strain hardening. Eq. (10) with Eq. (12) was formulated based on observations in the polycrystal plasticity predictions (Kuroda and Tvergaard, 2001a). A schematic illustration of Eq. (10) is shown in Fig. 1. If α is set to be unity (equivalently $c \equiv 0$), this corresponds to Simo's original proposition. The modification shown in Eqs. (10) and (12) may seem to be minor, but has a significant effect on predicted behavior. Although α is only slightly less than unity for usual elastic–viscoplastic materials, such a small deviation from unity has large effect on predictions of strain localization, as has been shown in Kuroda and Tvergaard (2001a) and will be shown later in this paper.

The Cauchy stress $\boldsymbol{\sigma}$ is related to the nominal stress $\boldsymbol{\Pi}$ through $\boldsymbol{\Pi} = J\mathbf{F}^{-1}\boldsymbol{\sigma}$, where $\mathbf{F}$ is the deformation gradient tensor and $J = \det\mathbf{F}$. When we choose the current configuration as a reference, the relationship between the nominal stress rate $\dot{\boldsymbol{\Pi}}$ and the material time derivative of Cauchy stress $\dot{\boldsymbol{\sigma}}$ is given by

$$\dot{\boldsymbol{\Pi}} = \dot{\boldsymbol{\sigma}} - \mathbf{L}\boldsymbol{\sigma} + (\mathrm{tr}\,\mathbf{L})\boldsymbol{\sigma}, \tag{13}$$

since we can set $\mathbf{F} = \mathbf{I}$, $J = 1$ and $\dot{J} = \mathrm{tr}\,\mathbf{L}$. This relation will be used in the finite element formulation shown below.

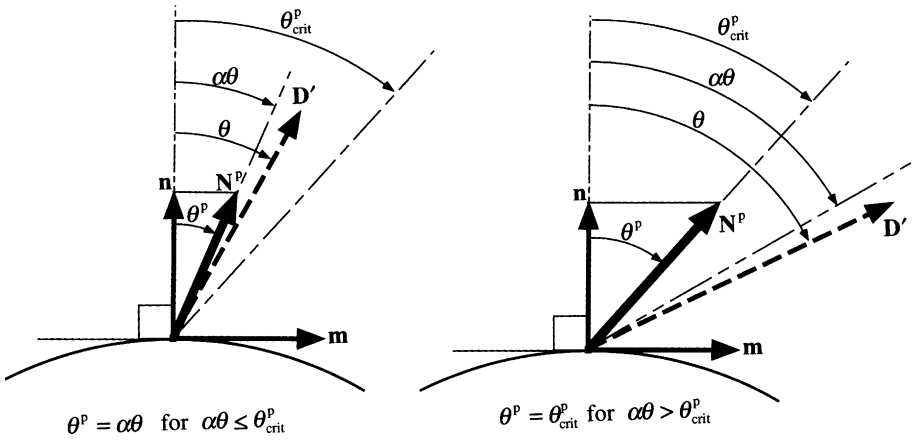

Fig. 1. Illustrations of the non-normality effect adopted in the present plasticity model.

2.2. Crystal plasticity

It is assumed that the elastic strain is small, but the plastic strain may be large. The crystal plasticity model used here is along the lines presented by Asaro (1979), Nemat-Nasser (1983), etc. In a single crystal, the velocity gradient $\mathbf{L}$ is decomposed into non-plastic and plastic parts,

$$\mathbf{L} = \mathbf{L}^{*} + \mathbf{L}^{p}. \tag{14}$$

The plastic contribution $\mathbf{L}^{p}$ is assumed to arise from slip on a finite number of slip systems,

$$\mathbf{L}^{p} = \mathbf{D}^{p} + \mathbf{W}^{p} = \sum_{\alpha} \dot{\gamma}^{(\alpha)} \mathbf{p}^{(\alpha)} + \sum_{\alpha} \dot{\gamma}^{(\alpha)} \mathbf{w}^{(\alpha)}, \tag{15}$$

where the superscript (α) represents a quantity with respect to the αth slip system, $\dot{\gamma}^{(\alpha)}$ is the slip rate of the αth slip system, $\mathbf{D}^{p}$ and $\mathbf{W}^{p}$ are the plastic rate of deformation and the plastic spin, respectively, and

$$\mathbf{p}^{(\alpha)} = \tfrac{1}{2}(\mathbf{s}^{(\alpha)} \otimes \mathbf{m}^{(\alpha)} + \mathbf{m}^{(\alpha)} \otimes \mathbf{s}^{(\alpha)}), \quad \mathbf{w}^{(\alpha)} = \tfrac{1}{2}(\mathbf{s}^{(\alpha)} \otimes \mathbf{m}^{(\alpha)} - \mathbf{m}^{(\alpha)} \otimes \mathbf{s}^{(\alpha)}). \tag{16a, b}$$

Here, $\mathbf{m}^{(\alpha)}$ is the unit vector normal to the slip plane and $\mathbf{s}^{(\alpha)}$ is the unit vector representing the slip direction in the corresponding slip plane.

The contribution $\mathbf{L}^{*}$ corresponds to the elastic lattice distortion. The elastic constitutive relation for a crystal is assumed to be

$$\overset{\circ}{\boldsymbol{\sigma}}{}^{*} = \dot{\boldsymbol{\sigma}} - \mathbf{W}^{*}\boldsymbol{\sigma} + \boldsymbol{\sigma}\mathbf{W}^{*} = \mathbf{C} : \mathbf{D}^{*}, \tag{17}$$

$$\mathbf{D}^{*} = \tfrac{1}{2}(\mathbf{L}^{*} + \mathbf{L}^{*\mathrm{T}}), \quad \mathbf{W}^{*} = \tfrac{1}{2}(\mathbf{L}^{*} - \mathbf{L}^{*\mathrm{T}}), \tag{18a, b}$$

where $\mathbf{C}$ represents the instantaneous crystal elasticity moduli. Denoting the Jaumann rate by $\overset{\nabla}{\boldsymbol{\sigma}}$, which is based on the total continuum spin $\mathbf{W}$, it follows from Eqs. (14)–(18a,b) that

$$\overset{\nabla}{\boldsymbol{\sigma}} = \dot{\boldsymbol{\sigma}} - \mathbf{W}\boldsymbol{\sigma} + \boldsymbol{\sigma}\mathbf{W} = \mathbf{C} : \mathbf{D} - \dot{\mathbf{P}}, \tag{19a}$$

$$\dot{\mathbf{P}} = \sum_{\alpha} \dot{\gamma}^{(\alpha)} (\mathbf{C} : \mathbf{p}^{(\alpha)} + \mathbf{w}^{(\alpha)}\boldsymbol{\sigma} - \boldsymbol{\sigma}\mathbf{w}^{(\alpha)}). \tag{19b}$$

The evolution laws of $\mathbf{s}^{(\alpha)}$ and $\mathbf{m}^{(\alpha)}$ are simply assumed to be

$$\dot{\mathbf{s}}^{(\alpha)} = \mathbf{W}^{*}\mathbf{s}^{(\alpha)}, \quad \dot{\mathbf{m}}^{(\alpha)} = \mathbf{W}^{*}\mathbf{m}^{(\alpha)}. \tag{20a, b}$$

The slip rate $\dot{\gamma}^{(\alpha)}$ is assumed to be given by the following viscoplastic power law:

$$\dot{\gamma}^{(\alpha)} = \dot{\gamma}_0 \mathrm{sgn}(\tau^{(\alpha)}) \left| \frac{\tau^{(\alpha)}}{g^{(\alpha)}} \right|^{1/m}, \quad \tau^{(\alpha)} = \mathbf{p}^{(\alpha)} : \boldsymbol{\sigma}, \tag{21}$$

where $\dot{\gamma}_0$ is a reference slip rate, $\tau^{(\alpha)}$ is the resolved shear stress and $g^{(\alpha)}$ is the current hardness of the αth slip system. The evolution equation for $g^{(\alpha)}$ is assumed to be

$$\dot{g}^{(\alpha)} = \sum_{\beta} h_{\alpha\beta} |\dot{\gamma}^{(\beta)}|. \tag{22}$$

A specific form of the slip hardening $h_{\alpha\beta}$ will be defined later.

As a model for polycrystals, an extended Taylor model (Asaro and Needleman, 1985) is adopted, in which the deformation in each grain is taken to be identical to the macroscopic deformation of the continuum, i.e. in the rate form, $\mathbf{L}^{(k)} = \mathbf{L}$, where $\mathbf{L}^{(k)}$ and $\mathbf{L}$ denote the grain and macroscopic velocity gradients, respectively, with the superscript (k) denoting the grain indices ($k = 1, \ldots, N$; N represents the total number of grains). Taking the volume fraction of each grain to be identical, the macroscopic stress, $\bar{\boldsymbol{\sigma}}$, is obtained from averaging the values over the total number of grains; i.e.

$$\bar{\boldsymbol{\sigma}} = \frac{1}{N} \sum_{k=1}^{N} \boldsymbol{\sigma}^{(k)}. \tag{23}$$

Based on this approach, the macroscopic (average) constitutive relation becomes

$$\overset{\nabla}{\bar{\boldsymbol{\sigma}}} = \dot{\bar{\boldsymbol{\sigma}}} - \mathbf{W}\bar{\boldsymbol{\sigma}} + \bar{\boldsymbol{\sigma}}\mathbf{W} = \overline{\mathbf{C}} : \mathbf{D} - \dot{\overline{\mathbf{P}}}. \tag{24}$$

The nominal stress rate $\dot{\boldsymbol{\Pi}}^{(k)}$ in the kth grain with respect to the current configuration is related to $\dot{\boldsymbol{\sigma}}^{(k)}$ through

$$\dot{\boldsymbol{\Pi}}^{(k)} = \dot{\boldsymbol{\sigma}}^{(k)} - \mathbf{L}\boldsymbol{\sigma}^{(k)} + (\mathrm{tr}\,\mathbf{L})\boldsymbol{\sigma}^{(k)}. \tag{25}$$

The volume average version of Eq. (25) is given by

$$\dot{\overline{\boldsymbol{\Pi}}} = \dot{\bar{\boldsymbol{\sigma}}} - \mathbf{L}\bar{\boldsymbol{\sigma}} + (\mathrm{tr}\,\mathbf{L})\bar{\boldsymbol{\sigma}}. \tag{26}$$

Substituting Eq. (24) into Eq. (26), we have

$$\dot{\overline{\boldsymbol{\Pi}}} = \overline{\mathbf{C}} : \mathbf{D} - \dot{\overline{\mathbf{P}}} + \mathbf{W}\bar{\boldsymbol{\sigma}} - \bar{\boldsymbol{\sigma}}\mathbf{W} - \mathbf{L}\bar{\boldsymbol{\sigma}} + (\mathrm{tr}\,\mathbf{L})\bar{\boldsymbol{\sigma}}, \tag{27}$$

which will be directly used in the finite element formulation as shown later. The average plastic rate of deformation $\overline{\mathbf{D}}^{\mathrm{p}}$ is defined in terms of $\mathbf{D}^{\mathrm{p}(k)}$ in the same manner as in Eq. (23), i.e. $\overline{\mathbf{D}}^{\mathrm{p}} = (1/N)\sum_{k=1}^{N} \mathbf{D}^{\mathrm{p}(k)}$. The macroscopic equivalent plastic strain is defined by $\bar{\varepsilon}^{\mathrm{p}} = \int ((2/3)\overline{\mathbf{D}}^{\mathrm{p}} : \overline{\mathbf{D}}^{\mathrm{p}})^{1/2} \mathrm{d}t$. This quantity, $\bar{\varepsilon}^{\mathrm{p}}$, will be used only for a purpose of visualization of computational results.

2.3. Specialization of the models

For the phenomenological non-normality model, the material is assumed to be isotropic in the present application. Here, J_{e} in Eq. (4) is identified with the Mises-type equivalent stress, i.e. $J_{\mathrm{e}} = ((3/2)\boldsymbol{\sigma}' : \boldsymbol{\sigma}')^{1/2}$. Thus, all tensor or vector structure variables, $\mathbf{s}_i$, are excluded. Furthermore, according to the discussion in Kuroda and Tvergaard (2001b), the plastic spin $\mathbf{W}^{\mathrm{p}}$ in Eq. (2) vanishes if the material is isotropic. Hence,

the spin $\boldsymbol{\omega}$ is identified with the continuum spin $\mathbf{W}$. Thus, the objective rate $\overset{\circ}{\boldsymbol{\sigma}}$ in Eq. (3) is identical to the Jaumann rate $\overset{\nabla}{\boldsymbol{\sigma}}$ based on $\mathbf{W}$.

Corresponding to the above specialization, polycrystals consisting of randomly oriented grains are considered for the crystal plasticity computations. Two types of crystal structure are considered: (i) b.c.c. crystal with 24 slip systems of the types $\{1\,1\,0\}\langle 1\,1\,1\rangle$ and $\{1\,1\,2\}\langle 1\,1\,1\rangle$, and (ii) f.c.c. crystal with 12 slip systems of the type $\{1\,1\,1\}\langle 1\,1\,0\rangle$. The crystal elasticity moduli tensor $\mathbf{C}$ in Eq. (17) is also assumed to be isotropic, as in the phenomenological non-normality theory.

3. Numerical procedure and problem formulation

In the computational procedure, the constitutive relation of the non-normality theory, Eq. (3), is re-written by use of a rate-tangent modulus method (Peirce et al., 1984), in order to perform stable numerical computations (see Kuroda and Tvergaard (2001a,b) for details). The present constitutive equation is non-linear for the rate of deformation $\mathbf{D}$. In Kuroda and Tvergaard (2001a) an iterative method was used for solving the non-linear equation. In the present application, the value of $\mathbf{D}$ used for constructing $\mathbf{N}^{\mathrm{p}}$ is taken to be the value determined in the previous increment without iteration. This is a good approximation as long as the increments are kept sufficiently small. The same kind of approximation has been employed in calculations with J_2 corner theory (Hutchinson and Tvergaard, 1981; Tvergaard et al., 1981). It has been confirmed that results for the non-normality theory, which will be shown in Section 4, have converged for reasonably chosen sizes of the increments.

Also for the crystal plasticity model, the rate tangent modulus method (Peirce et al., 1983) is applied to Eqs. (19a) and (19b). Furthermore, to accurately update the slip system vectors $\mathbf{s}^{(\alpha)}$ and $\mathbf{m}^{(\alpha)}$, the following technique for a finite time increment Δt is applied, instead of using the explicit rate forms in Eq. (20a,b), i.e.

$$\mathbf{s}^{(\alpha)}_{t+\Delta t} = \Delta\mathbf{R}^{*}\mathbf{s}^{(\alpha)}_{t}, \quad \mathbf{m}^{(\alpha)}_{t+\Delta t} = \Delta\mathbf{R}^{*}\mathbf{m}^{(\alpha)}_{t} \tag{28a, b}$$

with

$$\Delta\mathbf{R}^{*} = \mathbf{I} + \frac{\sin\omega}{\omega}\mathbf{W}^{*}\Delta t + \frac{1-\cos\omega}{\omega^{2}}\mathbf{W}^{*2}(\Delta t)^{2}, \quad \omega^{2} = -\frac{\mathrm{tr}[(\mathbf{W}^{*}\Delta t)^{2}]}{2}, \tag{29a, b}$$

which is based on a Taylor series under the assumption that $\mathbf{W}^{*}$ is constant during the time increment Δt.

An updated Lagrangian finite element formulation is employed. The finite element equation is derived on the basis of the rate-type principle of virtual work with neglect of the body force effect (e.g. McMeeking and Rice, 1975; Burke and Nix, 1979; Yamada and Sasaki, 1995)

$$\int_{V} \dot{\mathbf{\Pi}}^{\mathrm{T}} : \delta\mathbf{L}\,\mathrm{d}V = \int_{S_t} \dot{\mathbf{q}}\delta\boldsymbol{v}\,\mathrm{d}S, \tag{30}$$

where V and S are the current volume and surface, respectively, $\delta\boldsymbol{v}$ and $\delta\mathbf{L}$ are the virtual velocity and virtual velocity gradient, $\dot{\mathbf{q}}$ is the nominal rate of traction per unit current area of surface, and S_t is the surface over which the traction rates are prescribed. In the case of the polycrystal model, the nominal stress rate $\dot{\mathbf{\Pi}}$ is replaced by the 'average' one, $\overline{\dot{\mathbf{\Pi}}}$, in Eqs. (26) and (27).

The finite element equation is derived by substituting Eq. (13) with Eq. (3) or Eq. (27) into Eq. (30) and approximating the velocity field $\boldsymbol{v}$ in terms of finite element shape functions. The term $(\mathrm{tr}\,\mathbf{L})\boldsymbol{\sigma}$ in Eq. (13) or $(\mathrm{tr}\,\mathbf{L})\bar{\boldsymbol{\sigma}}$ in Eq. (27) results in a small non-symmetry of the geometric stiffness matrix in the finite element equation. But, this is not a disadvantage in the present computations for crystal plasticity, because the constitutive equation for crystal plasticity with the rate tangent modulus method (Peirce et al., 1983) itself is inherently non-symmetric.

Eight node isoparametric plane strain elements with four Gaussian integration points are used. In the case of the polycrystal model, the Taylor polycrystal model consisting of N grains is used in each Gaussian integration point.

A rectangular specimen is subjected to plane strain tension, with x_2 being the tensile axis. The initial dimensions of the specimen are $2H_0$ along the x_1-direction and $2L_0$ along the x_2-direction. Considering symmetric conditions, only one quadrant of the specimen is analyzed. Thus, the boundary conditions for the one quadrant are

$$v_1 = 0 \quad \text{and} \quad \dot{q}_2 = 0 \quad \text{on } X_1 = 0, \tag{31a}$$

$$v_2 = 0 \quad \text{and} \quad \dot{q}_1 = 0 \quad \text{on } X_2 = 0, \tag{31b}$$

$$\dot{q}_1 = \dot{q}_2 = 0 \quad \text{on } X_1 = H_0 + \Delta H_0, \tag{31c}$$

$$v_2 = \dot{U} \quad \text{and} \quad \dot{q}_1 = 0 \quad \text{on } X_2 = L_0, \tag{31d}$$

where X_i denotes the position of a material particle in the initial configuration, $\dot{U}$ is the prescribed rate of end-displacement, and ΔH_0 represents an initial geometrical imperfection, which is taken to be of the form (Tvergaard et al., 1981)

$$\Delta H_0 = H_0[-\xi_1 \cos(\pi X_2/L_0) + \xi_2 \cos(m_w \pi X_2/L_0)] \tag{32}$$

with ξ_1 and ξ_2 being imperfection amplitudes and m_w (>1) a wave number. The end-displacement is obtained from $U = \int \dot{U}\,\mathrm{d}t$. The problem formulation and the finite element mesh for one quadrant of the specimen to be analyzed are illustrated in Fig. 2. The initial aspect ratio of the specimen is taken to be $L_0/H_0 = 3$.

For the crystal plasticity calculations, polycrystals consisting of 48 grains, whose orientations have been randomly chosen, are employed. In Fig. 2, stereographic pole figures of $\{1\,1\,0\}$ for b.c.c. and of $\{1\,1\,1\}$ for f.c.c. are depicted.

The time increment Δt is determined so that $\Delta\varepsilon^p$ (or $\Delta\bar{\varepsilon}^p$) is always less than 0.002 in every integration point.

4. Numerical results

For the phenomenological non-normality model, the strain hardening function is taken to be given by

$$g(\varepsilon^p) = \sigma_0(1 + \varepsilon^p/\varepsilon_0)^n, \tag{33}$$

where σ_0 is the initial tensile yield strength, ε_0 is a material constant, and n is a strain hardening exponent. For the crystal plasticity model, the slip hardening rule is assumed to be

$$h_{\alpha\beta} = h = h_0\left(\frac{h_0\gamma_a}{\tau_0 n} + 1\right)^{n-1}, \quad \gamma_a = \int \sum_\alpha |\dot{\gamma}^{(\alpha)}|\,\mathrm{d}t, \tag{34a, b}$$

where h_0 is the initial slip hardening modulus, γ_a is an accumulated magnitude of slip, and τ_0 is the initial value of $g^{(\alpha)}$ for all the slip systems. The following values of the material constants are fixed throughout the present paper: $\sigma_0/\tau_0 = 2.8$, $E/\tau_0 = 1000$, $\nu = 0.3$, $h_0/\tau_0 = 30$, $n = 0.1$ and $\varepsilon_0 = 0.0015$. The rate of the end-displacement is prescribed as $\dot{U} = \dot{a}(L_0 + U)$ with $\dot{a} \equiv \dot{\Phi}_0$ or $\dot{\gamma}_0$. Also, the initial imperfection amplitude ξ_1 is always taken to be 0.005.

We first consider the behavior of a specimen with a pure cosine imperfection, where $\xi_2 = 0$. The rate sensitivity parameter is taken to be $m = 0.002$. The value of ε_0 for the non-normality model specified above

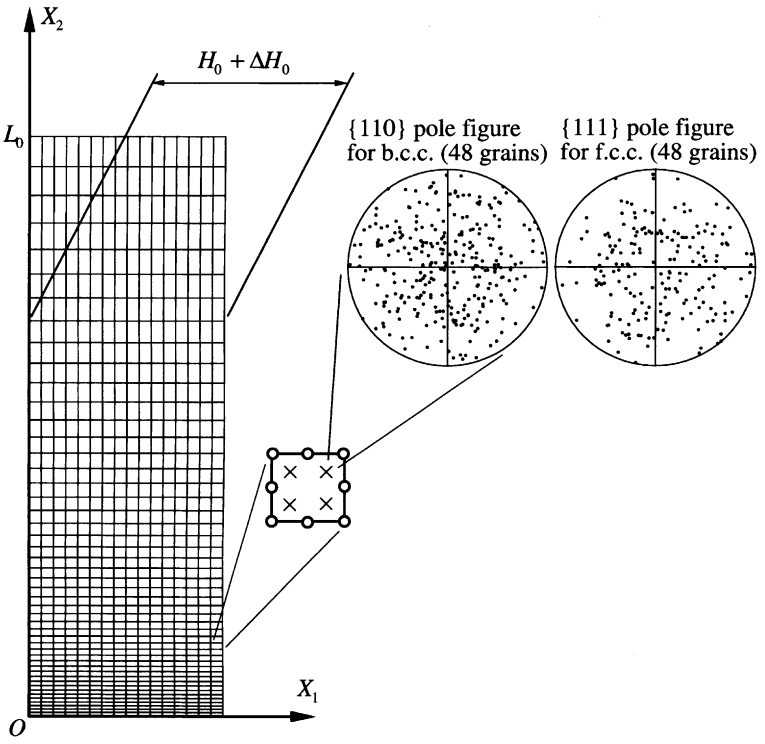

Fig. 2. Problem formulation of plane strain tensile test.

has been determined so that the load-elongation curves up to the attainment of the maximum load for the b.c.c. polycrystal model and for the non-normality model are close to each other (as seen in Fig. 3). For the non-normality model, two computations for $\theta^{p}_{crit} = 20°$ with $c = 0$ and 2 are performed.

Fig. 3 displays curves of the average nominal stress versus end-displacement. Here, the average nominal stress is defined by $\Pi_{ave} = P/H_0$, where P is the tensile load for one quadrant of the specimen, which is obtained by summation of the nodal forces in the X_2-direction at $X_2 = L_0$. The curve for the non-normality model with $c = 2$ is very close to that for the b.c.c. polycrystal model, even in the region where the load decays significantly. On the other hand, the curve for $c = 0$ exhibits a slightly lower maximum load, and deviates gradually from the curve for the b.c.c. model. The load curve for the f.c.c. model is higher than that for the b.c.c. This difference is attributed to the difference between the Taylor factors for the two crystal structures. The curve for the b.c.c. model reaches its maximum value, $\Pi_{ave}/\tau_0 = 4.50$, at $U/L_0 = 0.107$, while the curve for the f.c.c. model attains its maximum point, $\Pi_{ave}/\tau_0 = 4.88$, at $U/L_0 = 0.113$. However, the overall shape of the curve for the f.c.c. model is very similar to those for the b.c.c. model and the non-normality model with $c = 2$. It is noted that the computation time required for the b.c.c. model is one hundred and fifty times greater than that required for the non-normality model.

Fig. 4 illustrates deformed meshes at stages where shear bands have developed. Fig. 5 shows contours of the equivalent plastic strain, which correspond to the deformed meshes in Fig. 4. The patterns of the shear band formation for the non-normality model with $c = 2$, the b.c.c. and the f.c.c. are very similar to each other, although the width of the most narrow section (at the 'center' of the specimen) for the f.c.c. is slightly larger than that in the other two cases. The non-normality model with $c = 0$, which corresponds to the original proposal of Simo (1987), predicts a somewhat different pattern of shear band development,

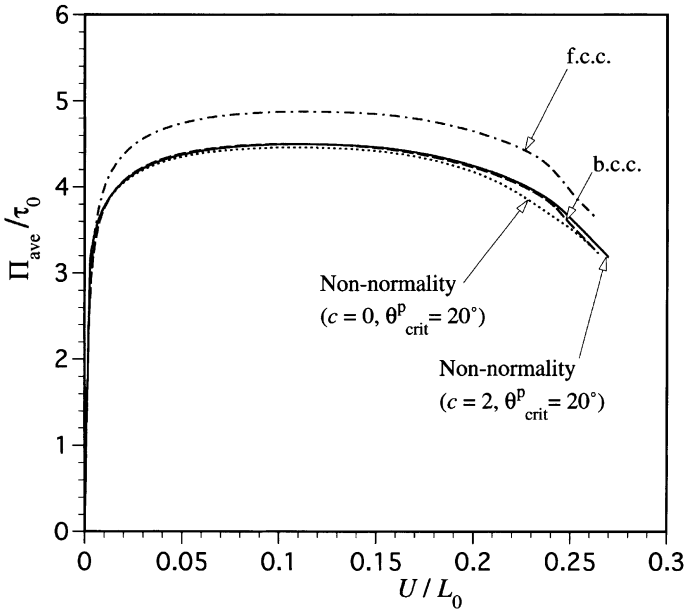

Fig. 3. Computed curves of tensile load versus end-displacement ($\xi_2 = 0$, $m = 0.002$).

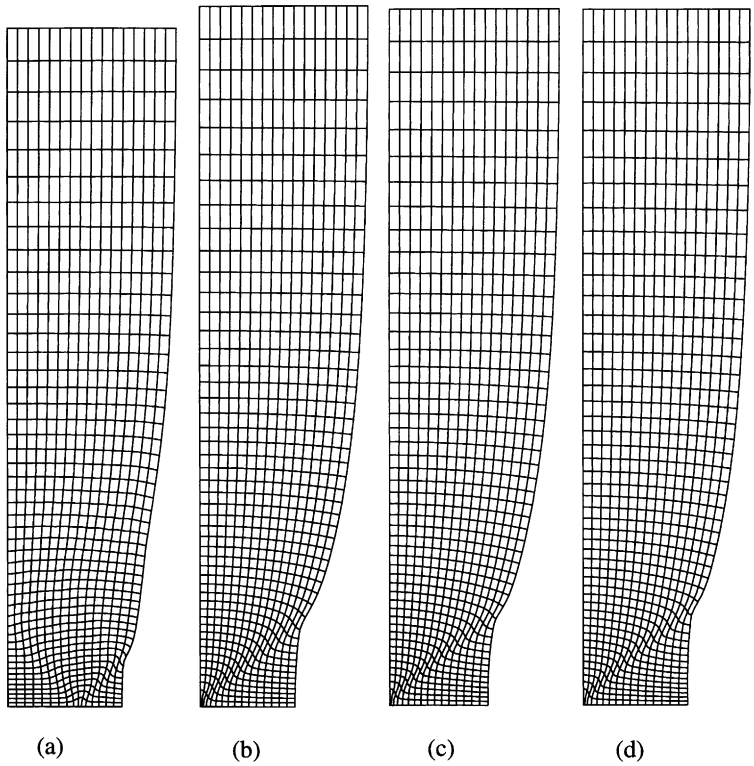

Fig. 4. Deformed meshes ($\xi_2 = 0$, $m = 0.002$): (a) non-normality model with $c = 0$ and $\theta^{p}_{crit} = 20°$ ($U/L_0 = 0.222$), (b) non-normality model with $c = 2$ and $\theta^{p}_{crit} = 20°$ ($U/L_0 = 0.260$), (c) b.c.c. ($U/L_0 = 0.255$) and (d) f.c.c. ($U/L_0 = 0.253$).

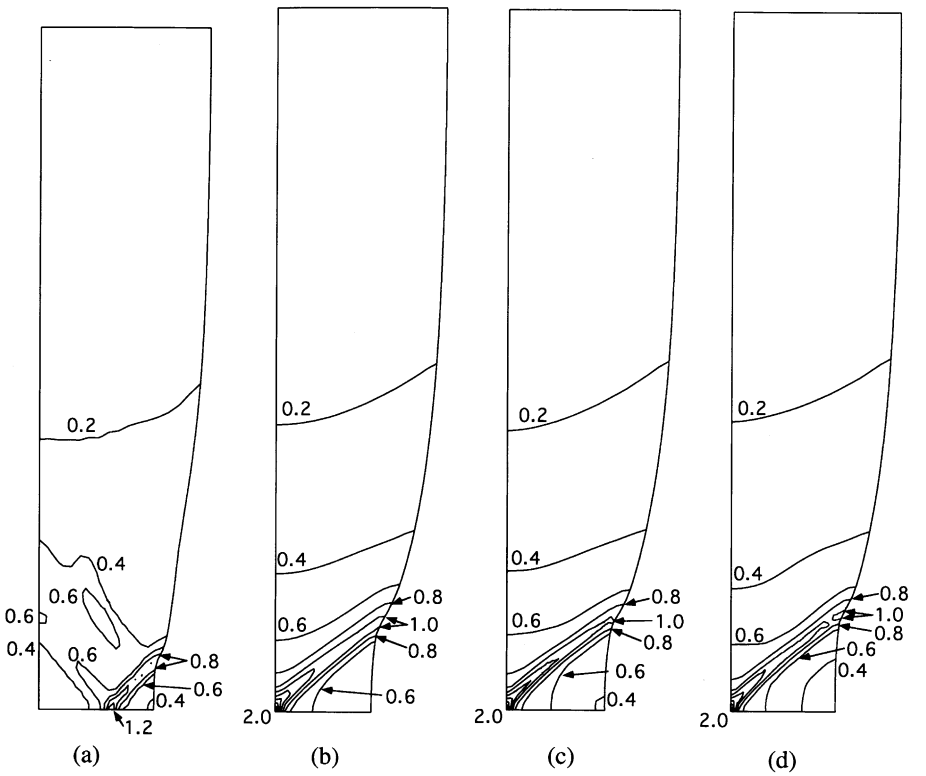

Fig. 5. Contours of equivalent plastic strain ε^{p} for non-normality model, or $\bar{\varepsilon}^{\mathrm{p}}$ for crystal plasticity model ($\xi_2 = 0$, $m = 0.002$): (a) non-normality model with $c = 0$ and $\theta^{\mathrm{p}}_{\mathrm{crit}} = 20°$, (b) non-normality model with $c = 2$ and $\theta^{\mathrm{p}}_{\mathrm{crit}} = 20°$, (c) b.c.c. and (d) f.c.c. These contours correspond to deformed meshes shown in Fig. 4.

representing two clear shear bands (due to the symmetry condition at $X_2 = 0$). It is interesting to note that the pattern of the shear band formation for the non-normality model with $c = 0$ is similar to some of the predictions for J_2 corner theory reported in Tvergaard et al. (1981, Fig. 5 on p. 129).

In Figs. 3–5, the critical (maximum) angle $\theta^{\mathrm{p}}_{\mathrm{crit}}$ of $\mathbf{D}^{\mathrm{p}}$ measured from the yield surface normal $\mathbf{n}$ was taken to be 20° which has been found to be a realistic value (Kuroda and Tvergaard, 2001a). Here, two additional calculations are performed for $\theta^{\mathrm{p}}_{\mathrm{crit}} = 5°$ and 45° with $c = 2$. All other parameter values are the same as those employed in Figs. 3–5. Curves of the average nominal stress versus end-displacement for $\theta^{\mathrm{p}}_{\mathrm{crit}} = 5°$, 20° and 45° are almost identical, although they are omitted here. Fig. 6 shows deformed meshes and contours of the equivalent plastic strain at stages where shear bands are visible for $\theta^{\mathrm{p}}_{\mathrm{crit}} = 5°$ and 45°. The intensity of the shear band development for $\theta^{\mathrm{p}}_{\mathrm{crit}} = 45°$ is almost identical to that for $\theta^{\mathrm{p}}_{\mathrm{crit}} = 20°$ (shown in Figs. 4 and 5), while the shear band for $\theta^{\mathrm{p}}_{\mathrm{crit}} = 5°$ is rather broad and less developed. It is understood from the findings in Fig. 6 that the choice of the value of c is of primary importance, while the predicted behavior of strain localization is less sensitive to the value of $\theta^{\mathrm{p}}_{\mathrm{crit}}$. The same tendency has been observed in the previous study based on the Marciniak–Kuczynski approach (see Kuroda and Tvergaard (2001a)).

In Figs. 7 and 8, a different imperfection mode is considered, i.e. $\xi_2 = 0.002$ and $m_{\mathrm{w}} = 4$. All other parameter values are the same as those employed in Figs. 3–5. The results for the non-normality model with $\theta^{\mathrm{p}}_{\mathrm{crit}} = 20°$ and $c = 2$ and for crystal plasticity models do not differ much from the corresponding results for $\xi_2 = 0$ (in Figs. 4 and 5). By contrast, the result for the non-normality model with $c = 0$ and $\theta^{\mathrm{p}}_{\mathrm{crit}} = 20°$ is strongly influenced by the change in the imperfection mode, such that a rather complex shear band pattern

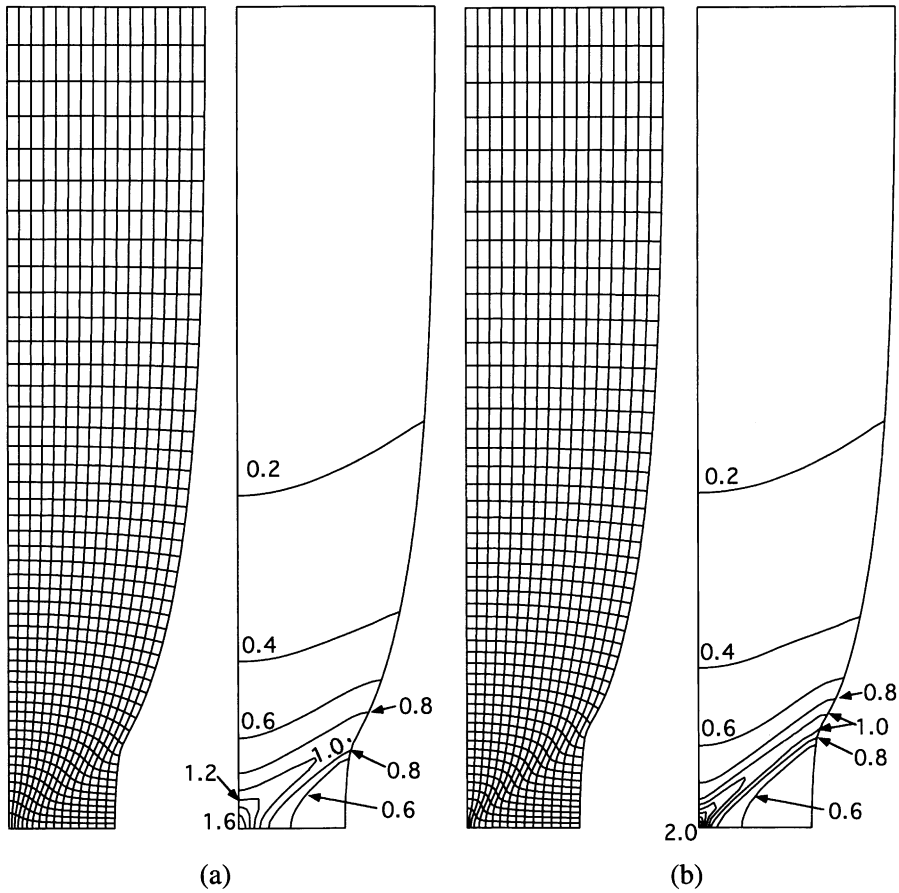

Fig. 6. Deformed meshes and contours of equivalent plastic strain ε^{p} for non-normality model ($\xi_2 = 0$, $m = 0.002$): (a) $c = 2$ with $\theta^{\mathrm{p}}_{\mathrm{crit}} = 5°$ ($U/L_0 = 0.263$) and (b) $c = 2$ with $\theta^{\mathrm{p}}_{\mathrm{crit}} = 45°$ ($U/L_0 = 0.260$).

and a broad shear zone are observed. The formation of the broad shear zone is somewhat similar to the prediction for J_2 corner theory reported in Tvergaard et al. (1981, Fig. 7 on p. 131).

Finally, several computations with a larger viscosity have been performed. Computations for the non-normality model with $c = 2$ and $\theta^{\mathrm{p}}_{\mathrm{crit}} = 20°$ and for the crystal plasticity models have been carried out for $m = 0.02$. Fig. 9 shows deformed meshes and contours of the equivalent plastic strain at stages where the neck is well developed. All other parameter values are the same as those employed in Figs. 3–5 and the pure cosine imperfection with $\xi_2 = 0$ is employed again. The results for the non-normality model and for the crystal plasticity models are very similar, but the width of the most narrow section for the f.c.c. is slightly wider than the other two cases. It is not clear that actual shear bands have developed here, or the bands are broader, even at $U/L_0 \approx 0.4$ for all the cases. The results shown here are consistent with the findings in many of previous studies, in which plastic instabilities are much delayed by an increase of viscosity.

5. Discussion

The basis for proposing the phenomenological plasticity model that combines a smooth yield surface for an anisotropic solid with a vertex-type plastic flow rule (Kuroda and Tvergaard, 2001a) was results of

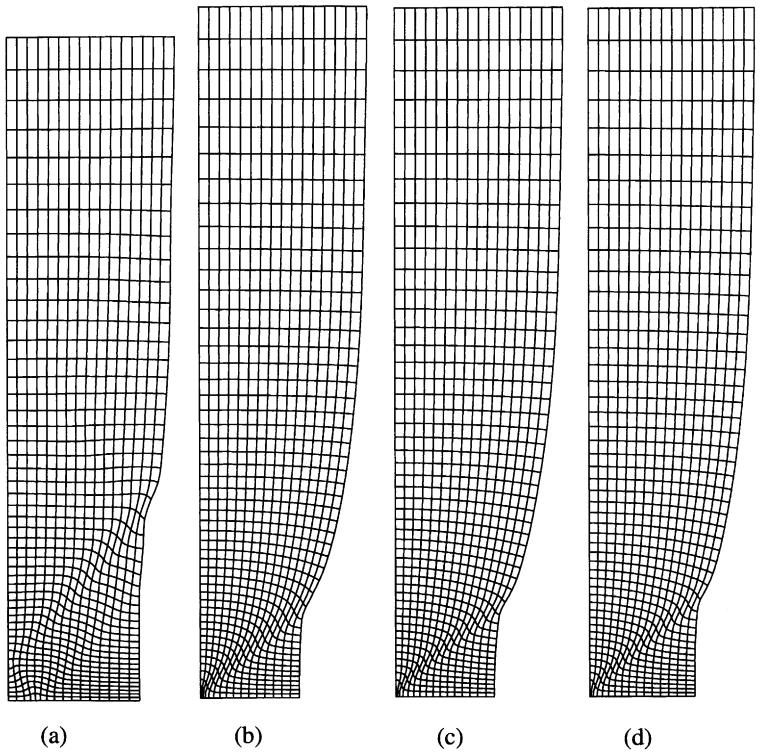

Fig. 7. Deformed meshes ($\xi_2 = 0.002$, $m_w = 4$, $m = 0.002$): (a) non-normality model with $c = 0$ and $\theta^{p}_{crit} = 20°$ ($U/L_0 = 0.204$), (b) non-normality model with $c = 2$ and $\theta^{p}_{crit} = 20°$ ($U/L_0 = 0.255$), (c) b.c.c. ($U/L_0 = 0.252$) and (d) f.c.c. ($U/L_0 = 0.250$).

Taylor model calculations for polycrystal plasticity, when using an abrupt strain path change to determine subsequent yield surface shapes (Kuroda and Tvergaard, 1999). The material parameters in this phenomenological model were tested by comparison with polycrystal plasticity predictions for the onset of necking in biaxially stretched metal sheets, according to the relatively simple M–K-type model. Also in the present paper the predictions of the phenomenological non-normality theory of plasticity has been tested against predictions for polycrystal plasticity, but here the comparison is made for the more complex problem of a full numerical solution of a boundary value problem, which involves first necking and then the formation of shear bands in the neck region, with subsequent evolution of highly localized shear deformations.

The non-normality model with $c = 0$ corresponds to the model of Simo (1987). The proposition of Simo (1987) focused on replacing the J_2 corner theory (Christoffersen and Hutchinson, 1979) by a simplified model more suitable for large scale computations. In this sense, the similarities between the results for $c = 0$ (in Figs. 4 and 7) and some results shown in Tvergaard et al. (1981) prove the soundness of the original idea of Simo. However, to reproduce the physically based crystal plasticity predictions, our improved theory is very efficient as seen in the previous section. In the present calculations, results which are closely consistent with the crystal plasticity predictions are obtained for $c = 2$. It is emphasized that the parameter c governing the non-coaxiality between $\mathbf{D}'$ and $\mathbf{D}^{p}$ has been introduced with the physical basis obtained from the observations in the crystal plasticity predictions (Kuroda and Tvergaard, 2001a). It is noted here that the strain localization predictions obtained by crystal plasticity are usually somewhat sensitive to a small change in initial grain orientations as, for example, seen in the M–K-model study (Kuroda and Tvergaard, 2001a).

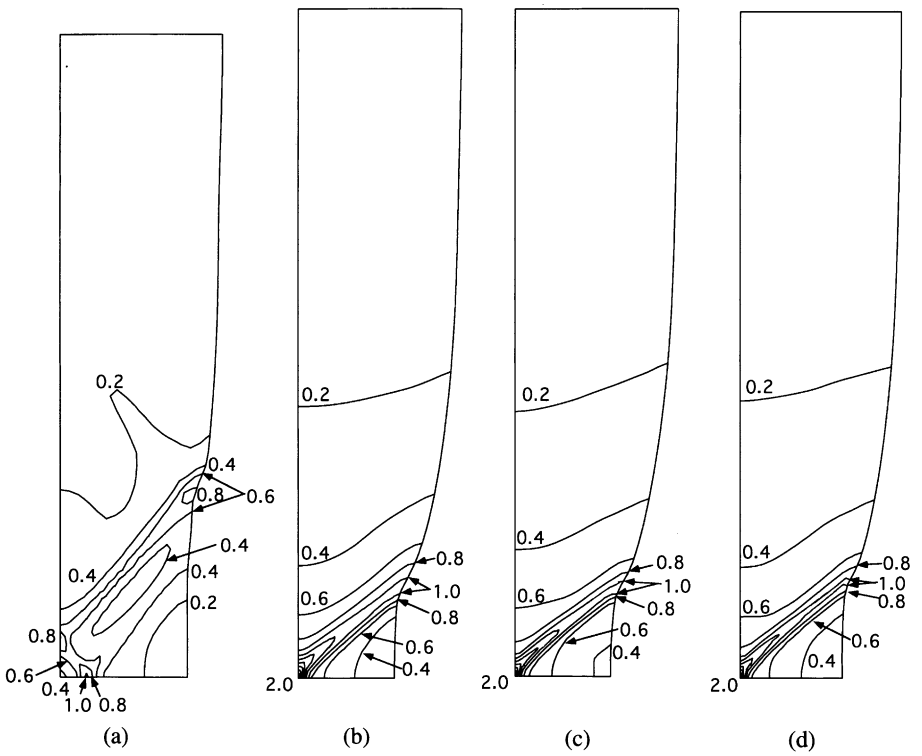

Fig. 8. Contours of equivalent plastic strain ε^{p} for non-normality model, or $\bar{\varepsilon}^{\mathrm{p}}$ for crystal plasticity model ($\xi_2 = 0.002$, $m_{\mathrm{w}} = 4$, $m = 0.002$): (a) non-normality model with $c = 0$ and $\theta^{\mathrm{p}}_{\mathrm{crit}} = 20°$, (b) non-normality model with $c = 2$ and $\theta^{\mathrm{p}}_{\mathrm{crit}} = 20°$, (c) b.c.c. and (d) f.c.c. These contours correspond to deformed meshes shown in Fig. 7.

Thus, the predicted shear band development may be slightly delayed or accelerated when a different set of 'random numbers' or different finite number of grains is employed. It is possible that a slightly different value of c would be more suitable for such a different case.

The eight noded isoparametric elements used for the present numerical analyses do not in general account for an abrupt jump in deformation gradient at the interface between shear band and surrounding material, as is the case for the so-called crossed triangles used in a number of shear band analyses (e.g. Tvergaard et al., 1981; Peirce et al., 1983). However, predictions based on crossed triangles are very sensitive to the shear band orientation relative to the mesh, while the type of elements used here show less sensitivity, as has been found in three dimensional analyses of Mathur et al. (1994). This ability to represent shear bands with an angle of inclination unknown a priori is important for a non-normality theory of plasticity with the possibility of plastic anisotropy, since the preferred orientation of shear bands is not known in advance.

The analyses of neck formation and shear band instabilities in polycrystalline materials, using the Taylor model for either b.c.c. or f.c.c. crystal structure, are presented here for the main purpose of illustrating the usefulness of predictions based on the phenomenological non-normality theory of plasticity. But these crystal plasticity analyses do represent new results, which have not been published before. It has been noted that the computation time required for some of these crystal plasticity analyses is one hundred and fifty times greater than that required for the non-normality model, which shows the efficiency of the phenomenological model. In relation to the present application of the Taylor model, accounting for 48 different

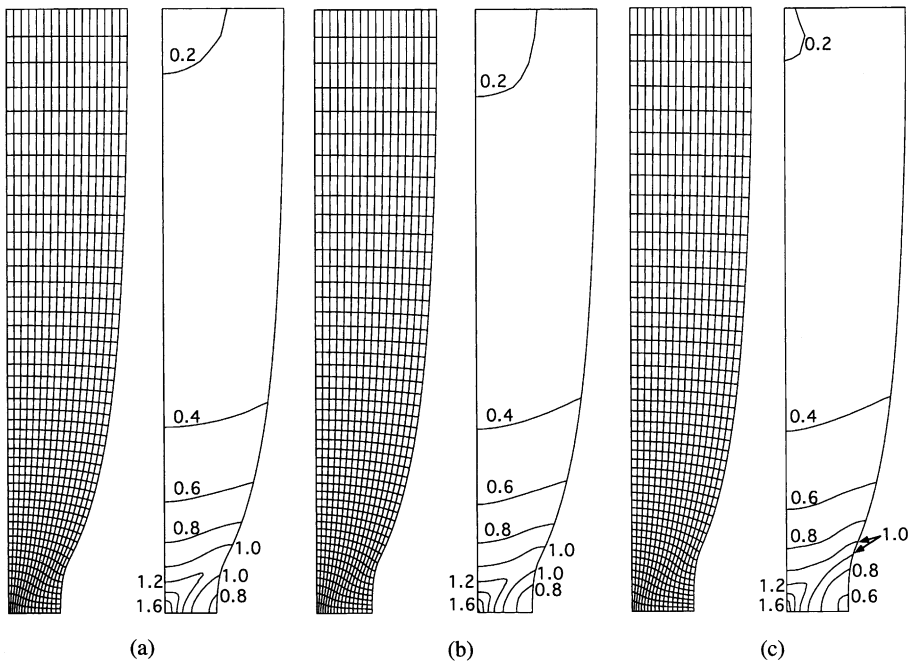

Fig. 9. Deformed meshes and contours of equivalent plastic strain ε^{p} for non-normality model, or $\bar{\varepsilon}^{\mathrm{p}}$ for crystal plasticity model ($\xi_2 = 0$, $m = 0.02$): (a) non-normality model with $c = 2$ and $\theta^{\mathrm{p}}_{\mathrm{crit}} = 20^\circ$ ($U/L_0 = 0.397$), (b) b.c.c. ($U/L_0 = 0.393$) and (c) f.c.c. ($U/L_0 = 0.393$).

grain orientations in each integration point, it is emphasized that this gives a reasonable approximation as long as the grain size is much smaller than the thickness of the tensile specimen, but not for grain sizes comparable to the thickness.

Although initial isotropy has been assumed for both the crystal plasticity and non-normality models, the crystal plasticity model naturally accounts for the subsequently induced anisotropy due to 'texture development'. By contrast, the present computations for the non-normality model do not include any effect of anisotropy. Nevertheless, the agreement was reasonable. But the non-normality model can account for initial anisotropy, as well as subsequently induced anisotropy, as presented in Kuroda and Tvergaard (2001a). In the general case of anisotropic material behavior in the non-normality theory of plasticity, it can be important to incorporate the effect of plastic spin, as has been discussed by Kuroda and Tvergaard (2001b). In addition, the computations performed in this paper were restricted to consider one quarter of a rectangular specimen. A main effect of considering only one quarter of the specimen is that we could not predict a single (unsymmetric) shear band, as is often observed in experiments. The effects of the anisotropy and the plastic spin, as well as the unsymmetric shear band formation, will be further studied in a forthcoming paper.

Acknowledgement

This work is partly supported by the Danish Technical Research Council in a project on Anisotropic Plasticity under the Materials Research Programme.

References

Asaro, R.J., 1979. Geometrical effects in the inhomogeneous deformation of ductile single crystals. Acta Metallurgica 33, 923–953.
Asaro, R.J., Needleman, A., 1985. Texture development and strain hardening in rate dependent polycrystals. Acta Metallurgica 33, 923–953.
Burke, M.A., Nix, W.D., 1979. A numerical study of necking in the plane strain tension test. Int. J. Solids Struct. 15, 379–393.
Christoffersen, J., Hutchinson, J.W., 1979. A class of phenomenological corner theories of plasticity. J. Mech. Phys. Solids 27, 465–487.
Gotoh, M., 1985. A simple plastic constitutive equation with vertex effect. Engng. Fract. Mech. 21, 673–684.
Hill, R., Hutchinson, J.W., 1975. Bifurcation phenomena in the plane tension test. J. Mech. Phys. Solids 23, 239–264.
Hu, P., Lian, J., Liu, Y.Q., Li, Y.X., 1998. A quasi flow corner theory of elastic–plastic finite deformation. Int. J. Solids Struct. 35, 1827–1845.
Hughes, T.R., Shakib, F., 1986. Pseudo-corner theory: a simple enhancement of J2-flow theory for applications involving non-proportional loading. Engng. Computat. 3, 116–120.
Hutchinson, J.W., Tvergaard, V., 1981. Shear band formation in plane strain. Int. J. Solids Struct. 17, 451–470.
Kuroda, M., Tvergaard, V., 1999. Use of abrupt strain path change for determining subsequent yield surface: illustrations of basic idea. Acta Materialia 47, 3879–3890.
Kuroda, M., Tvergaard, V., 2001a. A phenomenological plasticity model with non-normality effects representing observations in crystal plasticity. J. Mech. Phys. Solids 49, 1239–1263.
Kuroda, M., Tvergaard, V., 2001b. Plastic spin associated with a non-normality theory of plasticity, Eur. J. Mech. A/Solids (in press).
Kuwabara, T., Kuroda, M., Tvergaard, V., Nomura, K., 2000. Use of abrupt strain path change for determining subsequent yield surface: experimental study with metal sheets. Acta Materialia 48, 2071–2079.
Mathur, K.K., Needleman, A., Tvergaard, V., 1994. Ductile failure analyses on massively parallel computers. Comput. Meth. Appl. Mech. Engng. 119, 283–309.
McMeeking, R.M., Rice, J.R., 1975. Finite-element formulations for problems of large elastic–plastic deformation. Int. J. Solids Struct. 11, 601–616.
Neale, K.W., 1981. In: Phenomenological constitutive laws in finite plasticity, SM Archives, vol. 6. Sijthoff and Nordhoff Publishers, The Netherlands, pp. 79–128.
Needleman, A., Tvergaard, V., 1982. Aspects of plastic post-buckling behaviour. In: Hopkins, H.G., Sewell, M.J. (Eds.), Mechanics of Solids, The Rodney Hill 60th Anniversary Volume. Pergamon Press, Oxford, pp. 453–498.
Nemat-Nasser, S., 1983. On finite plastic flow of crystalline solids and geomaterials. J. Appl. Mech. 50, 1114–1126.
Peirce, D., Asaro, R.J., Needleman, A., 1983. Material rate dependence and localized deformation in crystalline solids. Acta Metallurgica 31, 1951–1976.
Peirce, D., Shih, C.F., Needleman, A., 1984. A tangent modulus method for rate dependent solids. Comput. Struct. 18, 875–887.
Simo, J.C., 1987. A J2-flow theory exhibiting a corner-like effect and suitable for large-scale computation. Comput. Meth. Appl. Mech. Engng. 62, 169–194.
Støren, S., Rice, J.R., 1975. Localized necking in thin sheets. J. Mech. Phys. Solids 23, 421–441.
Tvergaard, V., Needleman, A., Lo, K.K., 1981. Flow localization in plane strain tensile test. J. Mech. Phys. Solids 29, 115–142.
Yamada, Y., Sasaki, M., 1995. Elastic–plastic large deformation analysis program and lamina compression test. Int. J. Mech. Sci. 37, 691–707.